ChemElectroChem

Research Article
doi.org/10.1002/celc.202300429

Chemistry Europe
European Chemical Societies Publishing

www.chemelectrochem.org

Promotion of Direct Electron Transfer to Cytochrome c by Functionalized Thiophene-based Conducting Polymers

María J. Sáenz-Espinar,[a] Andrés F. Quintero-Jaime,[b] Alonso Gamero-Quijano,[a] Francisco Montilla,*[a] and Francisco Huerta[c]

Controlling direct electron transfer (DET) to redox proteins is of great interest for fundamental studies on biochemical processes and the development of biotechnological devices, such as biosensors or enzymatic fuel cells. Cytochrome c is a classical model protein for studying DET reactions that plays a key role in the onset of cellular apoptosis and the mitochondrial respiratory chain. In this contribution, we explored DET between cyt c and conducting polymers bearing the chemical structure of thiophene, specifically PEDOT, and its OH-containing derivative, PHMeEDOT. The combination of electrochemistry and *in situ* FTIR spectroscopy allowed us to gain more insight into the inner mechanism of DET at physiological pH. Hydrophilic interactions favour the correct orientation of the heme crevice of cytochrome c towards the polymer surface. When a positive charge is injected into the conducting polymer, the increasing electrostatic repulsion between protein and surface induces the desorption of lysine residues near the heme group and stimulates protein flipping. This effect was more pronounced at PEDOT- than PHMeEDOT-modified electrodes since the latter shows stronger interactions with lysine residues, partially hindering protein rotation at moderate potential. The potential-induced reorientation process was similar on both polymer surfaces, only at high positive potentials.

Introduction

Understanding the direct electron transfer from conducting materials to redox proteins is a current issue because of its latent interest in biochemistry and biotechnology.[1–3] Several reports have shown that the success of the charge transfer processes is highly dependent on the surface chemistry of the protein and its interfacial environment (e.g., electrode surface, local pH, electrolyte distribution).[4,5] Thus, the performance of several nanobiotechnological devices, such as electrochemical biosensors for health monitoring or enzymatic fuel cells, could be improved by identifying the specific amino acids involved in the redox reactions between proteins and conducting surfaces and which parameters might affect DET.[6–8]

[a] *M. J. Sáenz-Espinar, Dr. A. Gamero-Quijano, Prof. Dr. F. Montilla*
Departamento de Química Física e Instituto Universitario de Materiales de Alicante
Universidad de Alicante
Ado. de Correos 99, E-03080 Alicante (Spain)
E-mail: francisco.montilla@ua.es

[b] *Dr. A. F. Quintero-Jaime*
Bernal Institute and Department of Chemical Sciences
School of Natural Sciences
University of Limerick (UL)
Limerick V94 T9PX (Ireland)

[c] *Prof. Dr. F. Huerta*
Departamento de Ingenieria Textil y Papelera
Universitat Politecnica de Valencia
Plaza Ferrandiz y Carbonell, 1, E-03801 Alcoy (Spain)

Supporting information for this article is available on the WWW under https://doi.org/10.1002/celc.202300429

Among conductive materials, conducting polymers are conjugated systems capable of offering great versatility and biocompatibility for several biotechnological applications involving proteins.[9] These materials have already been used as electronic transducers in DNA biosensors or as active components in drug delivery systems.[10,11] Furthermore, due to their large surface area and straightforward synthesis, they have also been used as electroactive materials' scaffolds to ensure DET between electrodes and redox proteins such as glucose oxidase[12] or laccase[13] under native conditions. In particular, thiophene-based materials, which are electroactive at physiological pH, can host conductive nanostructures (gold nanoparticles, carbon nanotubes, graphene, etc.), facilitating DET between electrodes and proteins. However, few studies are focused on the structure of the polymer in the absence of additional components for this application.[14–17]

PEDOT, poly(3,4-ethylenedioxythiophene), one of the most biocompatible conducting polymers,[18] has been used to promote DET to proteins such as cytochrome c, enzymes, bacteria and neurons.[19–21] Poly(4-styrene sulfonate), PSS, which is extensively used as a dopant for PEDOT, enhances the solubility of the monomer in the polymerisation reaction, providing a permanent negative charge to the polymer and improves the processability of the synthesised material. However, recent studies have shown that the use of PSS as the dopant species could impair the performance of bioelectronic devices due to its influence on the local pH.[22]

On the other hand, Cyt c is a classical model protein for DET reactions in bioelectrochemistry[23–28] known for its crucial role in the onset of apoptosis and the mitochondrial respiratory chain.[29] This protein, which is almost spherical shape-like and about 3 nm in diameter, is located in the mitochondrial intermembrane space (IMM), where it plays the role of electron

carrier between cyt c reductase (Complex III) and cyt c oxidase (Complex IV).[30] Intensive research has shown that DET between Cyt c and bare solid electrodes is not easy to achieve as the redox-active heme centre is not exposed, and an appropriate orientation is required for the success of the process.[31,32] In addition, Cyt c adsorbs strongly on conventional metal electrodes,[33] which leads to undesired conformational changes in its tertiary structure (protein misfolding) and slow electron-transfer kinetics.[34,35]

Previous studies demonstrated that PEDOT doped with PSS facilitates DET to cyt c, with heterogeneous transfer constants significantly higher than those obtained with SAM-modified electrodes.[36–38] PEDOT-PSS favoured a proper orientation of the cyt c heme centre through electrostatic interactions between specific lysine residues at the protein and PSS sulfonate groups at the surface.[39] Since the presence of PSS could be misleading in the interpretation of charge transfer and other processes taking place at a molecular level, more studies on the interactions between surfactant-free polymers and proteins are required.

In the present contribution, we used two different surfactant-free thiophene-derived conducting polymers, PEDOT and PHMeEDOT (poly-hydroxymethyl-3,4-etylenedioxythiophene, Scheme 1). Both polymers were synthesised under similar conditions by electrochemical methods in organic solvent and afterwards tested for DET to the model protein cyt c in aqueous solutions. It is expected that the combination of voltammetric experiments with *in situ* FTIR spectroscopy can provide valuable information about the interfacial processes involved during DET, and how the chemical composition of the polymers is critical for inducing a proper orientation of the heme crevice during the charge transfer process.

Experimental

Cytochrome c from horse heart (98%), 3,4-ethylenedioxythiophene (97%), Hydroxymethyl-3,4-etylenedioxythiophene, acetonitrile (anhydrous), lithium perchlorate and deuterium oxide (99.9 atom % D) were purchased from Sigma-Aldrich. Potassium dihydrogen phosphate and dipotassium hydrogen phosphate were from Merck. All the reagents were of analytical grade. Aqueous solutions were prepared with ultrapure water obtained from an Elga Labwater Purelab system (18.2 MΩ cm). The phosphate buffer solution (PBS, pH 7) was a mixture of 0.15 M K_2HPO_4 + 0.10 M KH_2PO_4.

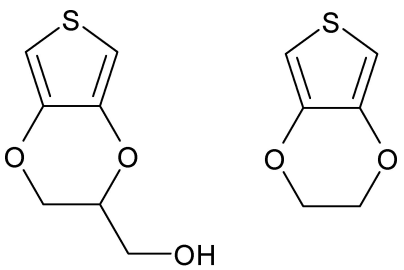

HMeEDOT EDOT

Scheme 1. Precursor monomers used in this work to obtain surfactant-free substrates for DET.

Cyclic voltammetry experiments were carried out using an EDAQ EA163 Potentiostat connected to a function generator (EG&G Parc model 175). The electrochemical cells were purged by bubbling N_2 for 20 min, and the inert atmosphere was maintained during all the experiments. In aqueous solutions, potentials were measured against a reversible hydrogen electrode (RHE, $E_{RHE} = -0.44$ V vs SHE) immersed in the medium. In organic solvent, the reference electrode was a silver wire pseudoreference. The pseudoreference electrode was calibrated with ferrocene added to the solution at the end of the voltammetric experiments. In all cases, a platinum wire was used as the counter electrode, and a 0.205 cm^2 polycrystalline platinum sphere was used as the working electrode. Prior to its use, the electrode surface was thermally cleaned in an air + propane flame. Finally, a droplet of ultrapure water protected the surface of the electrode.

X-ray photoelectron spectroscopy (XPS, K-ALPHA, Thermo Scientific) was used to analyse the sample's chemical composition. All spectra were collected using Al-K radiation (1486.6 eV), and a twin crystal monochromator, yielding a focused X-ray elliptical spot (major axis length of 400 μm) at 3 mA×12 kV. The alpha hemispherical analyser was operated in the constant energy mode with survey scan pass energies of 200 eV to measure the whole energy band and 50 eV in a narrow scan to selectively measure individual elements. XPS data were analysed with Avantage software. A smart background function was used to approximate the experimental backgrounds, and surface elemental composition was calculated from background-subtracted peak areas. Charge compensation was achieved with the system flood gun that provides low-energy electrons and low-energy argon ions from a single source. The experimental curves were adjusted using a combination of Lorentz (30%) and Gaussian (70%) functions.

In situ FTIR spectroscopy was performed in a Nicolet Thermo 5700 spectrometer equipped with a liquid nitrogen-cooled mercury-cadmium telluride, MCT, detector. The three-electrode spectroelectrochemical cell was equipped with a prismatic CaF_2 window bevelled at 60°. The working solution was bubbled with Ar flow for 20 min, and the inert atmosphere was maintained during the experiments. The counter electrode was a platinum ring, and a reversible hydrogen electrode (RHE) was used as the reference. The working electrode was a mirror-polished platinum disc. Prior to its use, the electrode surface was thermally cleaned as previously indicated.

In situ FTIR spectra were collected in the external reflection-absorption mode at 8 cm^{-1} resolution. Typically, 100 to 500 interferograms were processed with OMNIC data acquisition software to obtain both the background and the sample spectrum. The final spectra were expressed in the usual form, as the normalised difference between interferograms collected at sample and reference potentials: $\Delta R/R$. In these conditions, negative-going bands (downwards) are displayed when the corresponding vibrational modes appear or intensify at the sample potential, whereas a positive-going (upwards) means that the vibrational mode disappears or becomes IR-inactive at the sample potential. In this context, the surface selection rule predicts that some infrared absorption bands could weaken in the spectra of molecules attached to the metal surface, specifically those bands corresponding to molecular vibrations with an oscillating dipole moment parallel to the surface.

Results and Discussion

Synthesis and characterisation of polymer films

PEDOT and PHMeEDOT films were synthesised by cyclic scanning of the potential from solutions containing the corresponding precursor monomer. Figure 1A shows the first cyclic voltammogram recorded for a Pt electrode in the presence of EDOT monomer in acetonitrile solution. The forward scan shows a featureless curve until the potential reaches the mark of 0.6 V, corresponding to the oxidation onset of EDOT molecules. The positive limit potential was set at 0.85 V. Repetitive potential cycling led to the electrochemical growth of a PEDOT film, which was evidenced by the development of capacitative-like plateaus in the potential region between 0.0 V and 0.6 V (see Figure 1B). The polymerisation of HMeEDOT monomer was performed in a similar way (for more details see Figure S1 in the supporting information).

Polymers were grown until the current density reached 100 $\mu A\,cm^{-2}$ at 0.2 V, which corresponds to a polymer thickness of about 0.2 μm, as determined by the double-layer capacitance.[36,40]

Electrodes coated with the polymer layers were extracted from the organic solution, rinsed with abundant ultrapure water, dried, and characterised by X-ray-photoelectron spectroscopy (XPS) and scanning electron microscopy (SEM). The characterisation of both films is shown in FigureS2–S5 in the supporting information.

SEM images show slight differences in the surface morphology. Both materials presented compact deposits of similar texture fibres with bundles of about 0.1–0.2 microns in diameter. PEDOT films coated the electrode surface more evenly, although scattered amorphous agglomerates of about 10 to 20 microns with three-dimensional structures were observed. Regarding PHMeEDOT, more domains composed of aggregated fibres with substructures similar in shape and size to those found for PEDOT were observed.

The XPS survey spectra (Figures S3–S5 and Table S1) confirmed the presence of oxygen, sulphur and carbon for both materials and suggested that impurities were not significantly incorporated into the films. Both polymers present similar chemical compositions, but the analysis of the high-resolution C 1s spectrum (Figure S5) shows that the intensity of the C–O transition at 286.5 eV is enhanced for PHMeEDOT. Such a feature suggests the presence of more oxygenated functionalities on the surface of this material, as expected from its chemical structure (see Table S1).

The freshly deposited polymer films were also characterized by cyclic voltammetry experiments carried out in aqueous phosphate buffer solutions (PBS). Figure 2 A shows that PEDOT

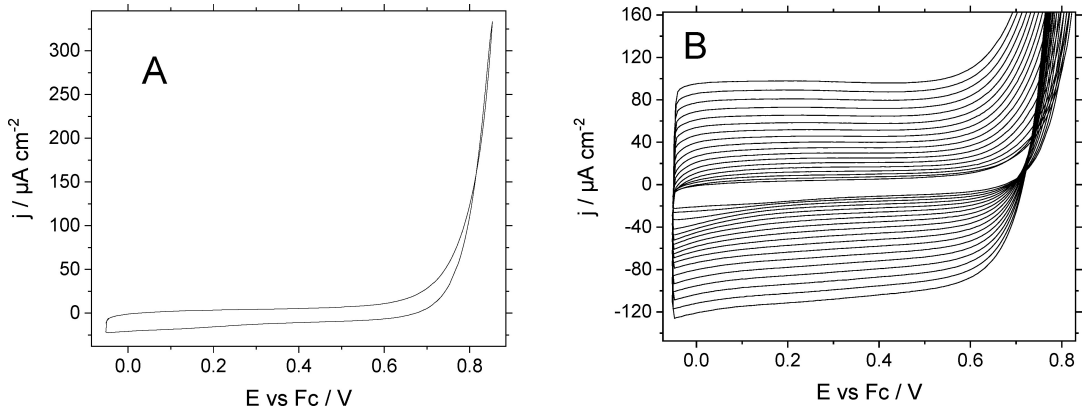

Figure 1. Cyclic voltammograms recorded during the potentiodynamic growth of a PEDOT film on a platinum electrode in an acetonitrile solution containing 0.01 M EDOT and 0.1 M $LiClO_4$. Scan rate 100 $mV\,s^{-1}$. **(A)** first voltammetric cycle; **(B)** successive potential scans.

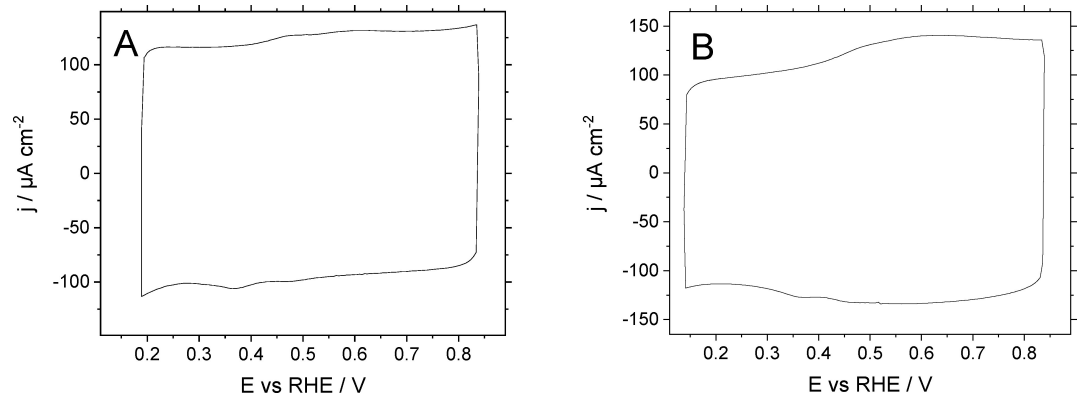

Figure 2. Stabilized CVs of **(A)** PEDOT and **(B)** PHMeEDOT electrodeposited on Pt electrodes in PBS solution at 100 $mV\,s^{-1}$.

does not undergo the transition from the non-conducting to the conducting state, typical of many conjugated polymers, since it is outside the potential window for solvent stability. Such behaviour is similar to that reported for PEDOT films doped with PSS[36] and means that the polymer will remain in its doped (conducting) state during all the experiments. With regard to PHMeEDOT films, the most remarkable point in the CV is the higher current intensity recorded at potentials above 0.4 V. Also, in this case, the non-conducting to conducting transition cannot be observed within the working potential window.

To confirm the capacitive character of the currents recorded in Figure 2, additional voltammetric studies were conducted at different scan rates (see Figures S6 and S7 in the supporting information). As expected for capacitive processes, recorded currents grow proportional to the scan rate applied for both polymers. PEDOT shows a double-layer capacitance close to 0.95 $\mu F\,cm^{-2}$, as determined by the slope of the plot current vs. scan rate (Figure S7B). Such a value remains constant regardless of the potential chosen for the study. However, PHMeEDOT's behaviour is slightly different above and below 0.4 V. A higher capacitance of approximately 1.22 $\mu F\,cm^{-2}$ is recorded for potentials higher than 0.4 V, whereas below this point, the recorded value drops to 1.05 $\mu F\,cm^{-2}$. The presence of hydrophilic groups in PHMeEDOT, which provide better access for the solvent electrolyte within the polymer matrix during potential cycling, seems to be the origin of the increased capacitance of this material.[41]

Each platinum electrode coated with the corresponding polymer film (PEDOT or PHMeEDOT) was transferred to the spectroelectrochemical cell and studied by *in situ* FTIR spectroscopy. The experiments were performed in deuterated water to avoid the interfering H_2O bending vibration band that usually appears between 1600–1700 cm^{-1} (see Figure S8 for experiments performed in non-deuterated aqueous solutions). Figure 3 shows the FTIR spectra at given potentials, highlighting the most significant vibrational peaks. Both polymer films show a negative-going band at around 1530 cm^{-1} when the potential reaches 0.3 V. Such a feature is assigned to the quinoid C_α—C_β antisymmetric stretching[42–44] whose intensity increases slightly upon oxidation and shifts towards higher wavenumbers. For PEDOT, this absorption peak shifts linearly at a rate close to $+25\ cm^{-1}V^{-1}$, akin to an electrochemical Stark effect. Ring-stretching vibrations of thiophene, typical of five-membered heterocycle compounds, appear in the form of two positive-going bands centred at 1470 and 1365 cm^{-1} for both materials. These vibrations suggest that, as potential swept towards positive values, the concentration of aromatic rings in the conjugated chain decreases as they transform into quinoid-like rings with deeper doping levels.[45]

In addition, two negative-going bands appear at 1420 and 1257 cm^{-1}, the former being attributed to the symmetric C–C stretching inside an EDOT moiety and the latter to the inter-ring C=C symmetric stretching.[36,44] Vibrational modes coming from C–S bonds in thiophene rings should appear at frequencies out of the CaF_2 vibrational window and, consequently, are undetectable in these experiments. As expected, the spectroelectrochemical behaviour of PHMeEDOT was similar to that of PEDOT, since the pendant hydroxymethyl moieties are out of the conjugated backbone. The most remarkable difference is observed in the position and intensity of the band assigned to the inter-ring C–C stretching vibration, which appears at a higher energy for PHMeEDOT. In addition, the electrochemical Stark shift of the quinoid band is slightly higher (about 30 $cm^{-1}V^{-1}$) than for PEDOT.

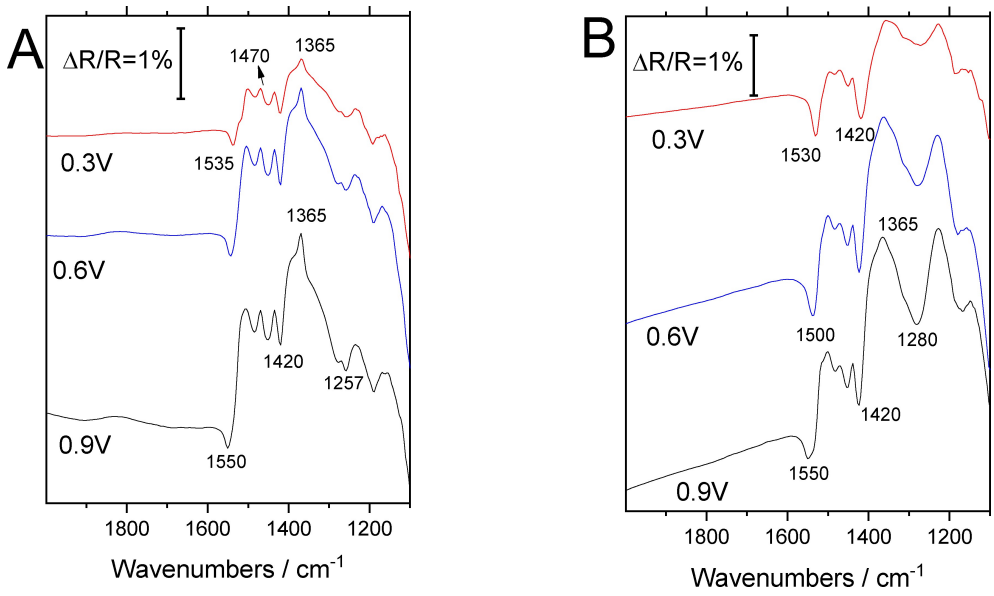

Figure 3. *In situ* FTIR spectra collected in PBS-D_2O for **(A)** PEDOT and **(B)** PHMeEDOT electrodeposited films. Sample potentials are indicated in the figure. The reference spectra were obtained at 0.1 V and 100 interferograms were collected at each potential.

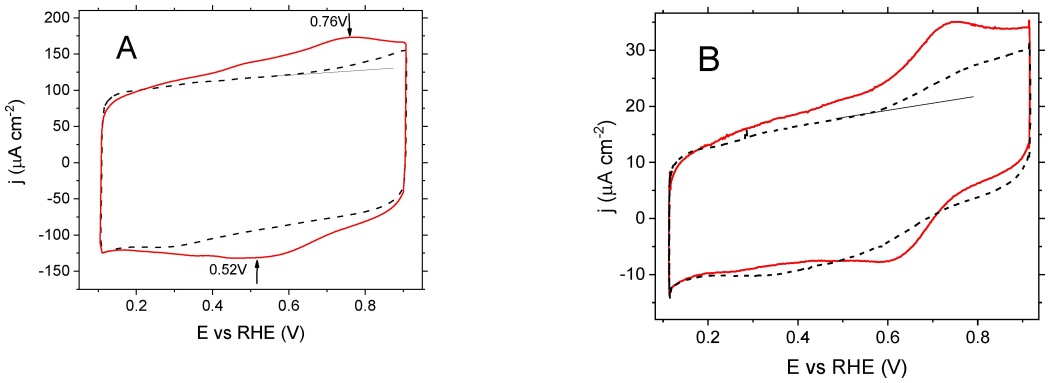

Figure 4. CVs recorded for polymer-modified electrodes in PBS solution at **(A)** 100 mV s^{-1} and **(B)** 10 mV s^{-1} in the presence of cyt c (5 mg mL^{-1}). Dashed line: PEDOT-modified electrode. Solid line: PHMeEDOT-modified electrode.

Direct electron transfer from polymer films to cyt c

The charge transfer process between cyt c and the polymer-coated surfaces was characterized electrochemically by means of cyclic voltammetry in H_2O/PBS. In Figure 4, a comparison is made between CVs recorded at different scan rates for PEDOT (dashed line) and PHMeEDOT (solid line) in the presence of cyt c (5 mg mL^{-1}).

At high scan rate (Figure 4A), the electrode coated with PEDOT presented a capacitive current during the forward scan up to ca. 0.6 V. Above this potential, a slight positive net current can be observed related to cyt c oxidation, although the concomitant reduction wave cannot be clearly distinguished in the reverse sweep. The redox processes undergone by the protein appear better defined at the PHMeEDOT surface (solid red line in Figure 4A). The anodic peak centred at around 0.76 V in the forward scan is attributed to the oxidation of the heme group of the protein: cyt c-Fe(II)→cyt c-Fe(III). The corresponding counter process, cyt c-Fe(III)→cyt c-Fe(II), appears as a broad reduction current peaking at around 0.52 V. The obtained cyt c half-wave potential agrees with typical values reported in the literature.[46–48] When the potential is scanned at low rates (Figure 4B) both coated electrodes can record the redox process undergone by cyt c, although the electrochemical response is still better defined at the hydroxylated polymer. For that surface, the anodic peak stands at 0.75 V, whereas the cathodic wave shifts 60 mV towards positive peaking at 0.58 V. As a result, the peak separation at low scanning rates drops to 170 mV. For PEDOT, decreasing the scan rate improves the voltammetric wave corresponding to cyt c oxidation, although the reverse scan shows an ill-defined reduction peak centred at 0.32 V. Therefore, cyclic voltammetry results confirm that the hydroxylated polymer exhibits better electrocatalytic performance for the electron transfer to cyt c in terms of both, electrochemical reversibility and redox current recorded. A more in-depth study on the effects of scan rate on the voltammetric response of polymer-cyt c systems is presented in the supplementary information. Figure S9 shows (supporting information) that polymer film capacitive current drops linearly by decreasing the scan rate. Besides, Randles-Sevcik plots (Figure S10 in the supporting information) reveal almost parallel, straight lines for the electron transfer (faradic current), which can be interpreted in terms of a similar DET mechanism at both polymer surfaces.

In situ FTIR spectroscopy was used to gain more insight into the direct electron transfer process between cyt c and polymer-modified electrodes. The presence of protein in the working solution results in significant spectral changes within the 1500–1800 cm^{-1} region compared to Figure 3. In the first spectroscopic experiment, the upper potential limit was set at 0.6 V to ensure that cyt c remained in its reduced state (Figure 5).

The assignments of major bands detected in these FTIR (and in the subsequent) experiments are compiled and summarized in Table 1.

Under these conditions, the cyt c-Fe(II) infrared spectra recorded at PEDOT (Figure 5A) are dominated by a broad,

Table 1. Assignment of *in situ* FTIR main bands for the reduced and the oxidised cyt c forms of the protein in the 1500–1800 cm^{-1} spectral region.

Assignment	Reduced	Oxidised	Source	Residues
Amide I	1685	1675	β-turn type III	14–17, 67–70
	1658	1662	β-turn type II	21–24, 32–38, 75–78
		1643	Disordered chain	18–20, 25–31, 41–48, 79–87
	1632	1635	β-strand	37–40, 57–59
Heme υ_{37}	1590	1608	Heme $C_\beta C_\beta$	
Amide II		1550	β-turn type III	14–19, 67–70
Tyrosine	1515		in-plane ring vibration	67

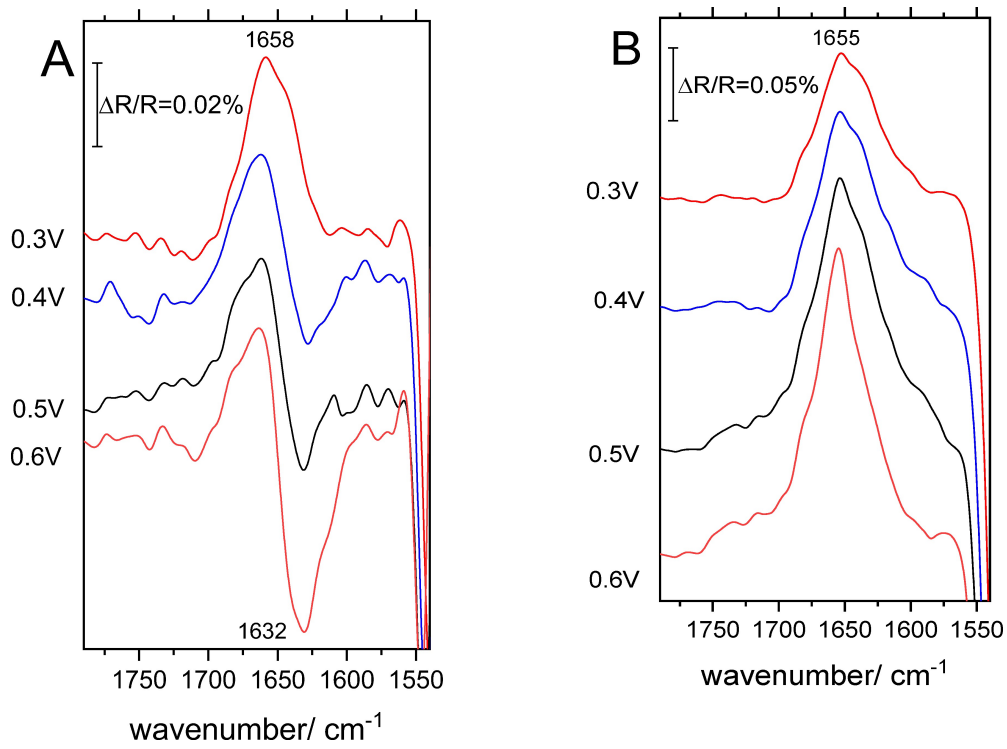

Figure 5. *In situ* FTIR spectra obtained in the presence of cyt c (5 mg mL^{-1}) for **(A)** PEDOT and **(B)** PHMeEDOT films. The reference spectrum was collected at 0.1 V and the sample potentials are indicated in the figure. 100 interferograms at each potential.

positive absorption band peaking at around 1658 cm^{-1}. The main contribution to this band comes from amide I vibrations within the β-turn type II region of cyt c,[49] although the shoulder at lower energy may indicate absorption from peptides located in α-helix and disordered domains.[50] The positive character of the 1658 cm^{-1} feature is attributed either to partial desorption or to its reorientation (that drives to an inactivation of the IR-mode) at the sample potential.

Above 0.4 V an additional negative band assigned to β-strand residues[51,52] emerges at 1632 cm^{-1}. The intensity of this absorption rises at higher potentials, thus suggesting that cyt c interactions with the PEDOT surface change progressively under the influence of an increasing interfacial electric field. Since β-strand residues are located on the backside of the protein (opposite to the heme crevice, see Scheme S1 in the supporting information), the intensification of this absorption band reveals a protein reorientation, a flipping of cyt c. The persistence of the positive band at 1658 cm^{-1} at these potentials points either to a slight desorption or to a reorientation of the protein induced by the positive charge inserted into the polymer backbone. It is worth mentioning that the lack of infrared features coming from β-turn type III at around 1690 cm^{-1} strongly suggests that hydrophilic interactions between reduced cyt c and the PEDOT surface prevail over hydrophobic interactions.[51]

The *in situ* FTIR spectra of PHMeEDOT (Figure 5B) show some similarities with those of PEDOT, but also some interesting differences. The absence of features around 1690 cm^{-1} suggests that hydrophilic interactions are dominant, the presence of the positive band of amide I peaking at 1655 cm^{-1} showing contributions from α-helix regions.[50] As for PEDOT, the increasing intensity of the 1655 cm^{-1} feature in the spectra of Figure 5B reveals that α-helix and β-turn contributions become progressively weaker at increasing potential, an effect that can be attributed either to a minor desorption or to a reorientation of the protein. The major difference of this series of spectra compared to PEDOT is the lack of negative-going β-strand absorptions in the surroundings of 1630 cm^{-1} supports the absence of flipping, at least in the range of potentials for which the reduced form of the protein predominates. The stronger interaction between the OH-terminated PHMeEDOT and the positively charged lysine residues, mostly located near the heme crevice, could be at the origin of the differences with the PEDOT-cyt c system.

The spectroscopic responses of both protein-polymer systems at potentials of 0.7 V and above, for which the more stable protein form is the oxidised structure cyt c-Fe(III), are depicted in Figure 6.

The redox transition of the iron centre, Fe (II)→Fe (III), is confirmed by the appearance of two additional bands peaking at 1608 cm^{-1} (negative) and 1590 cm^{-1} (positive), both related to the υ_{37} vibrational modes of the heme group. Along with these absorptions, a new positive-going band appears at 1685 cm^{-1} for both films. Such a feature seems closely related to a downward element peaking at 1675 cm^{-1}, more apparent for PEDOT but also present for PHMeEDOT. This pair of bands are assigned to vibrational modes involving β-turn type III residues and, in addition, the bipolar character can be related

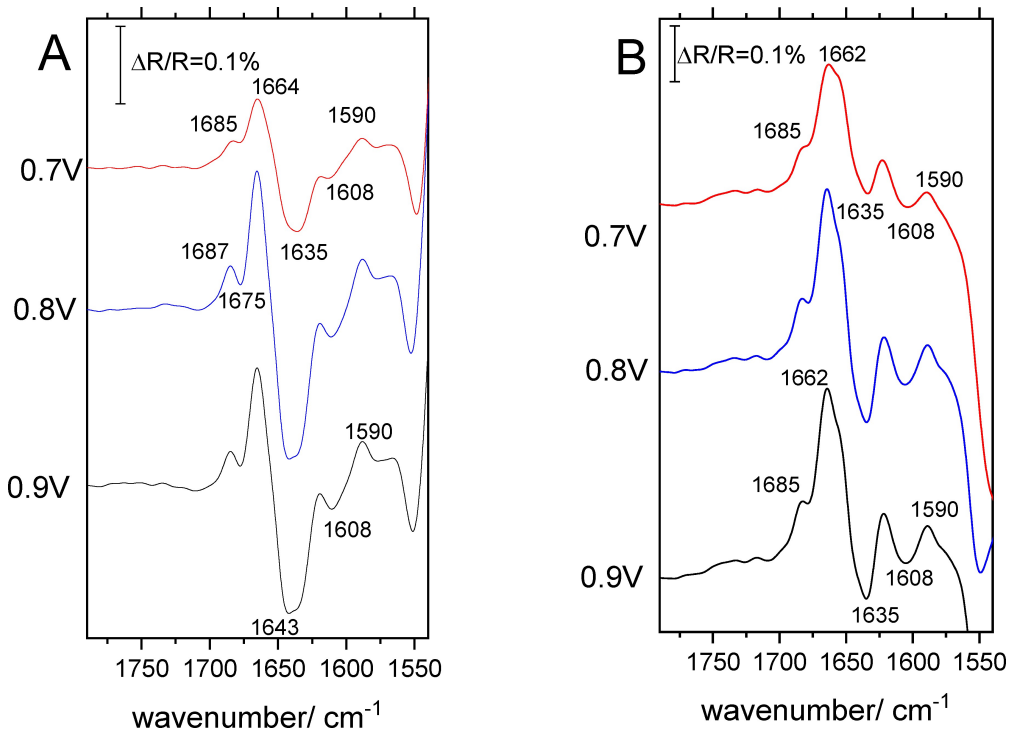

Figure 6. *In situ* FTIR spectra collected for **(A)** PEDOT and **(B)** PHMeEDOT films in the presence of cyt c (5 mg mL^{-1}). Reference potential was 0.1 V in all cases and sample potential is indicated for each spectrum. 100 interferograms collected at each potential.

to changes in the redox state of cyt c: on the one hand, the negative-going component at 1675 cm^{-1} reports the loss of cyt c-Fe(II) and, on the other, the positive-going part at 1685 cm^{-1} shows the advent of the oxidised form, cyt c-Fe(III). Since the protein residues involved in β-turn type III are 14–17 and 67–70 (see Table 1), which are bordering the protein heme crevice, the bipolar character of this feature suggests the occurrence of a close interaction between the heme centre and the polymer surface in this range of potentials, as depicted in Scheme S2 in the supporting information.

The increasing intensity of the upward band at around 1662 cm^{-1} in Figure 6 also demonstrates that the interaction between β-turn type II residues and the surface of both polymers weakens at increasing potential. Such a behaviour is similar to that described for the reduced cyt c-Fe(II) form in Figure 5. In this context, it is worth recalling that the negative absorption at 1632 cm^{-1} suggested the protein flipping on PEDOT below 0.7 V, a feature not detectable on PHMeEDOT under parallel experimental conditions. In contrast, this negative band appears in all the spectra of Figure 6B, thus proving that cyt c reorientation is not suppressed at the more hydrophilic polymer surface.

The progress of the flipping process was monitored for both polymer substrates in Figure 7A by plotting the intensity of the corresponding 1632–1635 cm^{-1} absorption against the applied potential.

From this graph, it can be concluded that the rotation of the reduced form, cyt c-Fe(II), is hindered on PHMeEDOT but takes place gradually on PEDOT at increasing potentials. This response agrees with the voltammetric results in Figure 4C, where a higher oxidation current was recorded at lower potentials for PHMeEDOT. The evidence that the hydroxyl-terminated polymer prevents the early flipping of cyt c, suggests that the number of protein molecules with the heme group facing the surface is more significant than on PEDOT. This improved response is attributed to a better interaction between the surface hydroxyl groups of PHMeEDOT and the positively charged lysine residues around the heme group (see the scheme of Figure 7), which is a key factor for proper electron transfer to the protein (Lys 13, 27, 72, 86).[53]

Furthermore, compared to cyt c-Fe(II), the flipping of cyt c-Fe(III) takes place at both polymers from 0.6 V, occurs at approximately the same rate and completes at around 0.8-0.9 V.

The minimization of spectral interferences coming from the redox transitions of polymers is key to correctly interpreting spectroscopic features related explicitly to DET. Therefore, to improve the signal-to-noise ratio of such bands, the applied potential was restricted around the cyt c redox process, with five consecutive potential steps done between 0.5 V and 0.7 V. Using the so-called SNIFTIR technique, each sample spectrum obtained at 0.7 V was referred to that collected previously at 0.5 V and after 5 cycles, the resulting spectra were averaged to obtain an improved resolution for the cyt c redox transition. The averaged spectra of PEDOT and PHMeEDOT substrates are shown in Figure 8. First, it should be noted that the negative band at 1635 cm^{-1} is overlapped with a higher frequency feature peaking at 1643 cm^{-1} and assigned to amide I vibrations coming from disordered regions. The relative intensity of the latter component is higher for PEDOT, but the opposite is true for PHMeEDOT, which suggests a different protein orientation

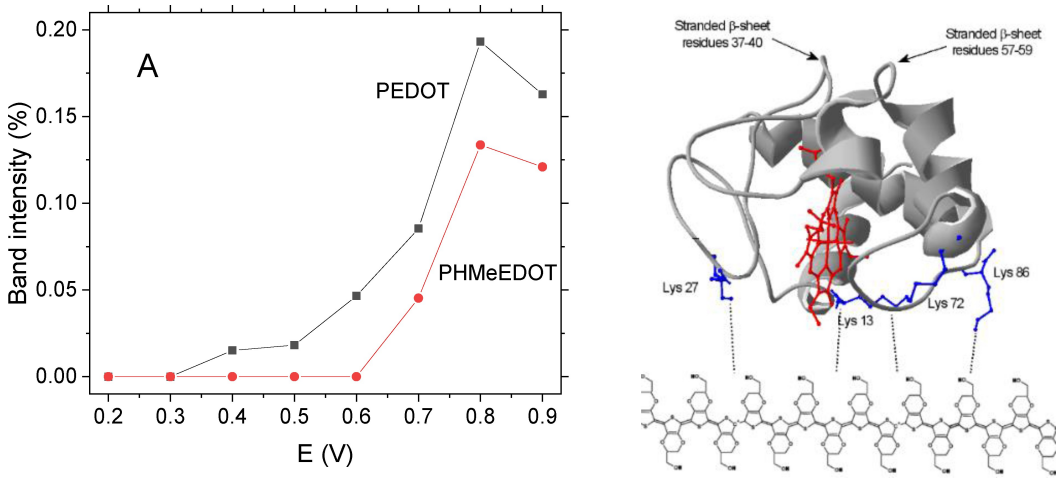

Figure 7. (A) Potential dependence of the band intensity from the negative absorption coming from β-strand (1632–1635 cm^{-1}) at PEDOT (black squares) and PHMeEDOT (red circles). The scheme shows Cyt c ribbon structure created with Swiss PDB Viewer 4.1.0 with crystallographic data taken from the Protein Data Bank (PDB ID 1HRC). Heme group marked in red and key lysines marked in blue.

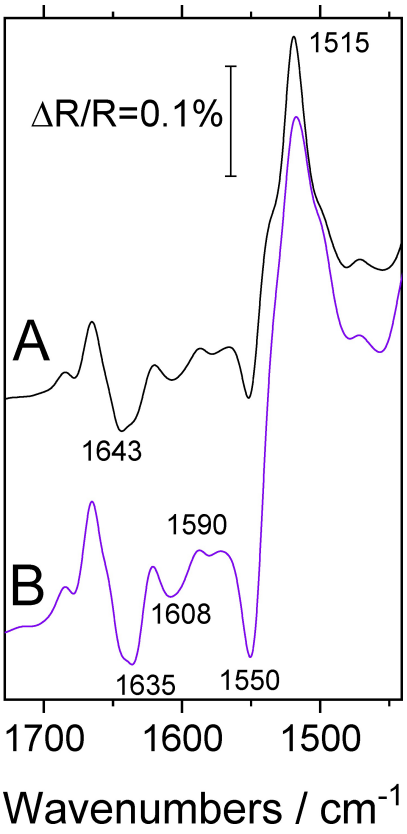

Figure 8. *In situ* SNIFTIR spectra collected for (**A**) PEDOT and (**B**) PHMeEDOT films in the presence of cyt c (5 mg mL^{-1}). Reference potential 0.5 V, sample potential 0.7 V. 500 interferograms alternatively collected at each potential.

at the sample potential and also at the end of the flipping process.

Another evident difference between the two spectra of Figure 8 lies in the enhanced intensities of the negative absorption at 1550 cm^{-1} and the positive one at 1515 cm^{-1} for PHMeEDOT. Although the polymer's own infrared transitions may still distort both bands, the former can be assigned to the amide II transition of the β-turn type III in the protein, whereas the positive feature at 1515 cm^{-1} corresponds to the in-plane ring vibration of tyrosine 67. Both bands should be strongly affected by the redox state and orientation of the protein since the tyrosine residue is located inside the heme hydrophobic pocket (see Scheme S3 in the supporting information), and the β-turn type III comprises several peptides located close to the heme crevice (see Scheme S2 in the supporting information).

The positive character of the band related to tyrosine 67 indicates the vanishing of the associated vibrational mode, either by desorption of the heme group from the surface or by a tilt of the corresponding dipole moment, making it more parallel to the surface. The negative character of the transition related to the β-turn type III implies that this mode reactivates during the oxidation process. Therefore, desorption due to oxidation can be ruled out, and protein reorientation after oxidation seems a more reliable explanation. The fact that these bands are more intense for the OH-terminated polymer suggests a higher proportion of proteins with the heme group near the surface flipping upon oxidation. This interpretation is also supported by the suppressed rotation of cyt c below 0.6 V on this substrate.

Conclusions

The direct electron transfer between PEDOT or PHMeEDOT surfaces and cytochrome c was investigated at physiological pH by a combination of electrochemical and vibrational spectroscopy techniques. To facilitate the interpretation of the vibrational spectra and to avoid interference with the DET process, both polymeric materials were electrochemically synthesised in the absence of surfactant species.

The hydroxymethyl group of PHMeEDOT is located outside the conjugated backbone. As a result, the spectroelectrochemical behaviour of PEDOT and PHMeEDOT was similar. Further-

more, no significant differences in the morphology of the deposited films were observed.

It was found that the orientation of the protein over the electrode surface depends on the positive charge injected into the polymer substrate. In this way, the downward infrared absorption at 1635 cm^{-1} coming from the β-strand at the opposite side of the heme centre was used to monitor the potential-induced flipping. At potentials lower than those required to oxidise cyt c, the protein shows more freedom of movement, and thus of realignment, on PEDOT. However, under similar experimental conditions, a minor amount of cyt c-Fe(II) molecules could desorb from the PHMeEDOT surface and no reorientation was detected. The stronger interactions of positively charged Lys residues with this OH-terminated (and thus more hydrophilic) substrate seem at the origin of the different behaviour observed. Therefore, hydrophilic interactions between cyt c and the conducting polymer substrate constitute a key factor for DET, as the heme crevice must be oriented towards the electrode surface during electron transfer.

The oxidised form of cyt c, which predominates at potentials above 0.65 V, reorientates faster and nearly at the same rate on both polymer surfaces, with the flipping process being completed at 0.8 V. This result suggests that electrostatic interactions between polymer and protein may be altered by the redox state of the heme centre.

Acknowledgements

Financial support by Spanish Ministry of Science (projects TED2021-129894B-I00 and PDC2021-120884-I00), Generalitat Valenciana (projects GVA-THINKINAZUL/2021/015, MFA/2022/058 and CIPROM/2021/62) and European Union (NextGenerationEU PRTR-C17.I1) is gratefully acknowledged. A.G.-Q. acknowledges funding received from his Marie Skłodowska-Curie Postdoctoral Fellowship (Grant Number MSCA-IF-EF-ST 2020/101018277).

Conflict of Interests

The authors declare no conflict of interest.

Data Availability Statement

The data that support the findings of this study are available from the corresponding author upon reasonable request.

Keywords: Conducting polymer · cytochrome c · direct electrochemistry · flipping · PEDOT · redox protein

[1] F. A. Armstrong, A. O. Hill, N. J. Walton, *Acc. Chem. Res.* **1988**, *21*, 407–413.
[2] C. Leger, P. Bertrand, *Chem. Rev.* **2008**, *108*, 2379–2438.
[3] D. W. M. Arrigan, M. J. Hackett, R. L. Mancera, *Curr. Opin. Electrochem.* **2018**, *12*, 27–32.
[4] D. Ivnitski, B. Branch, P. Atanassov, C. Apblett, *Electrochem. Commun.* **2006**, *8*, 1204–1210.
[5] J. J. Gooding, R. Wibowo, J. Liu, W. Yang, D. Losic, S. Orbons, F. J. Mearns, J. G. Shapter, D. B. Hibbert, *J. Am. Chem. Soc.* **2003**, *125*, 9006–9007.
[6] R. A. Bullen, T. C. Arnot, J. B. Lakeman, F. C. Walsh, *Biosens. Bioelectron.* **2006**, *21*, 2015–2045.
[7] D. Leech, P. Kavanagh, W. Schuhmann, *Electrochim. Acta* **2012**, *84*, 223–234.
[8] L. Gorton, A. Lindgren, T. Larsson, F. D. Munteanu, T. Ruzgas, I. Gazaryan, *Anal. Chim. Acta* **1999**, *400*, 91–108.
[9] S. Tajik, H. Beitollahi, F. G. Nejad, I. S. Shoaie, M. A. Khalilzadeh, M. S. Asl, Q. Van Le, K. Zhang, H. W. Jang, M. Shokouhimehr, *RSC Adv.* **2020**, *10*, 37834–37856.
[10] M. Gerard, A. Chaubey, B. D. Malhotra, *Biosens. Bioelectron.* **2002**, *17*, 345–359.
[11] D. Svirskis, J. Travas-Sejdic, A. Rodgers, S. Garg, *J. Controlled Release* **2010**, *146*, 6–15.
[12] S. Thakur, A. Verma, W. F. Alsanie, G. Christie, V. K. Thakur, *Mater. Lett.* **2022**, *307*, 130971.
[13] Q. Pan, Q. Wu, Q. Sun, X. Zhou, L. Cheng, S. Zhang, Y. Yuan, Z. Zhang, J. Ma, Y. Zhang, B. Zhu, *Sens. Actuators B* **2022**, *373*, 132703.
[14] W. C. Alvin Koh, M. A. Rahman, E. S. Choe, D. K. Lee, Y. B. Shim, *Biosens. Bioelectron.* **2008**, *23*, 1374–1381.
[15] M. Eguílaz, L. Agüí, P. Yáñez-Sedeño, J. M. M. Pingarrón, *J. Electroanal. Chem.* **2010**, *644*, 30–35.
[16] H. J. Kim, K. S. Lee, M. S. Won, Y. B. Shim, *Langmuir* **2008**, *24*, 1087–1093.
[17] M. H. Naveen, N. G. Gurudatt, Y. B. Shim, *Appl. Mater. Today* **2017**, *9*, 419–433.
[18] R. A. Lehane, A. Gamero-Quijano, S. Malijauskaite, A. Holzinger, M. Conroy, F. Laffir, A. Kumar, U. Bangert, K. McGourty, M. D. Scanlon, *J. Am. Chem. Soc.* **2022**, *144*, 4853–4862.
[19] J. Park, H. K. Kim, Y. Son, *Sens. Actuators B* **2008**, *133*, 244–250.
[20] P. Santhosh, K. M. Manesh, S. Uthayakumar, S. Komathi, A. I. Gopalan, K. P. Lee, *Bioelectrochemistry* **2009**, *75*, 61–66.
[21] T. J. Zajdel, M. Baruch, G. Méhes, E. Stavrinidou, M. Berggren, M. M. Maharbiz, D. T. Simon, C. M. Ajo-Franklin, *Sci. Rep.* **2018**, *8*, 15293.
[22] J. Rivnay, S. Inal, A. Salleo, R. M. Owens, M. Berggren, G. G. Malliaras, *Nat. Rev. Mater.* **2018**, *3*.
[23] F. A. Armstrong, G. S. Wilson, *Electrochim. Acta* **2000**, *45*, 2623–2645.
[24] M. Collinson, E. F. Bowden, M. J. Tarlov, *Langmuir* **1992**, *8*, 1247–1250.
[25] E. F. Bowden, F. M. Hawkridge, H. N. Blount, *J. Electroanal. Chem. Interfacial Electrochem.* **1984**, *161*, 355–376.
[26] T. Sagara, K. Niwa, A. Sone, C. Hinnan, K. Niki, *Langmuir* **1990**, *6*, 254.
[27] M. J. Eddowes, H. A. Hill, *J. Am. Chem. Soc.* **1979**, *101*, 4461–4464.
[28] G. A. Mines, T. Pascher, S. C. Lee, J. R. Winkler, H. B. Gray, *Chem. Biol.* **1996**, *3*, 491–497.
[29] A. Gamero-Quijano, S. Bhattacharya, P.-A. A. Cazade, A. F. Molina-Osorio, C. Beecher, A. Djeghader, T. Soulimane, M. Dossot, D. Thompson, G. G. Herzog, M. D. M. D. Scanlon, *Sci. Adv.* **2021**, *7*, 1–12.
[30] L. Wang, D. H. Waldeck, *J. Phys. Chem. C* **2008**, *112*, 1351–1356.
[31] X. Chen, H.-Y. Long, W.-L. Wu, Z.-S. Yang, *Thin Solid Films* **2009**, *517*, 2787–2791.
[32] Y. Zhou, J. Zhi, Y. Zou, W. Zhang, S.-T. Lee, *Anal. Chem.* **2008**, *80*, 4141–6.
[33] L. Wang, E. Wang, *Electrochem. Commun.* **2004**, *6*, 49–54.
[34] C. Hinnen, R. Parsons, K. Niki, *J. Electroanal. Chem. Interfacial Electrochem.* **1983**, *147*, 329–337.
[35] D. E. Reed, F. M. Hawkridge, *Anal. Chem.* **1987**, *59*, 2334–2339.
[36] S. López-Bernabeu, F. Huerta, E. Morallón, F. Montilla, *J. Phys. Chem. C* **2017**, *121*, 15870–15879.
[37] S. A. Mozaffari, T. Chang, S. M. Park, *J. Phys. Chem. C* **2009**, *113*, 12434–12442.
[38] D. Millo, A. Ranieri, W. Koot, C. Gooijer, G. Van Der Zwan, *Anal. Chem.* **2006**, *78*, 5622–5625.
[39] S. López-Bernabeu, A. Gamero-Quijano, F. Huerta, E. Morallón, F. Montilla, *J. Electroanal. Chem.* **2017**, *793*, 34–40.
[40] J. Bobacka, A. Lewenstam, A. Ivaska, *J. Electroanal. Chem.* **2000**, *489*, 17–27.
[41] L. Li, J. Meng, M. Zhang, T. Liu, C. Zhang, *Chem. Commun.* **2022**, *58*, 185–207.
[42] M. Łapkowski, A. Proń, *Synth. Met.* **2000**, *110*, 79–83.
[43] V. Hernandez, F. J. Ramirez, T. F. Otero, J. T. Lopez Navarrete, *J. Chem. Phys.* **1994**, *100*, 114–129.
[44] S. Garreau, J. L. Duvail, G. Louarn, *Synth. Met.* **2002**, *125*, 325–329.

[45] D. W. Mayo, in *Course Notes Interpret. Infrared Raman Spectra*, John Wiley & Sons, Inc., Hoboken, NJ, USA, **2004**, pp. 101–140.
[46] F. L. Rodkey, E. G. Ball, *J. Biol. Chem.* **1950**, *182*, 17–28.
[47] A. Gamero-Quijano, G. Herzog, M. D. Scanlon, *Electrochem. Commun.* **2019**, *109*, 106600.
[48] D. B. Craig, E. R. Nichols, *J. Chem. Educ.* **2006**, *83*, 1325–1326.
[49] T. Heimburg, D. Marsh, *Biophys. J.* **1993**, *65*, 2408–2417.
[50] M. Ye, Q. L. Zhang, H. Li, Y. X. Weng, W. C. Wang, X. G. Qiu, *Biophys. J.* **2007**, *93*, 2756–2766.
[51] K. Ataka, J. Heberle, *J. Am. Chem. Soc.* **2004**, *126*, 9445–9457.
[52] K. Ataka, J. Heberle, *J. Am. Chem. Soc.* **2003**, *125*, 4986–4987.
[53] S. Lin, X. Jiang, L. Wang, G. Li, L. Guo, *J. Phys. Chem. C* **2012**, *116*, 637–642.

Manuscript received: August 25, 2023
Revised manuscript received: October 16, 2023
Version of record online: November 13, 2023